

26

27 Abstract

28 ~~The determination of~~ Determining whether a cloud will evolve into a thunderstorm is
29 beneficial for understanding thunderstorm formation and is also important for ensuring the safety
30 of society. However, a clear understanding of the microphysics ~~in~~of clouds ~~for~~in terms of the
31 occurrence of lightning activity has not been attained. Vast field observations and laboratory
32 experiments indicate that graupel, which is rimed ice, is a vital hydrometeor for lightning
33 generation, and is the foundation of riming electrification. In this study, polarimetric radar and
34 lightning observations are used to compare the ice microphysics associated with graupel between
35 57 isolated thunderstorms and 39 isolated non-thunderstorms, and the differences in radar
36 parameters are quantified. Our results for the occurrence of lightning activity in clouds
37 ~~showed~~revealed the following results: 1) the maximum difference in graupel volume ~~at~~at the
38 -10°C isotherm height between thunderstorms and non-thunderstorms reached approximately 7.6
39 km^3 ; 2) the graupel particles approached spherical shapes with a mean differential reflectivity (Z_{DR})
40 value of 0.3 dB, which likely indicated that heavily rimed graupel was present; 3) the median
41 values of horizontal reflectivity (Z_{H}) or Z_{DR} at positions where the source initiation and channel of
42 the first lightning flashes were nearly 31 dBZ or 0 dB; and 34) 98.2% of the thunderstorms were
43 equipped with ~~the~~a Z_{DR} column, and the mean depth was ~ 2.5 km. Our study deepens our
44 understanding of lightning physics and thunderstorm formation.

45 Short summary

46 Understanding lightning activity is important for meteorology and atmospheric chemistry.
47 However, the occurrence of lightning activity in clouds is uncertain. In this ~~This~~ study, we
48 quantified the difference between isolated thunderstorms and non-thunderstorms. ~~Here we~~We
49 showed that lightning activity was more likely to occur with more graupel volume and/or ~~more~~
50 riming. ~~And a~~A deeper Z_{DR} column was associated with lightning occurrence. This information
51 can aid in a deeper understanding of lightning physics.

52 **Keywords:** thunderstorm; lightning; riming; cloud microphysics

53

54 **1. Introduction**

55 Thunderstorms are typically severe convection clouds. Lightning is not only a severe
56 weather hazard produced by thunderstorms but also a clear signature ~~of~~~~to mark the~~ thunderstorm
57 formation (MacGorman and Rust, 1998). Understanding lightning activity (especially for the first
58 lightning flash, ~~indicating~~which indicates the start of lightning activity in a cloud) is important
59 for understanding ~~the~~ meteorological processes, and the formation of thunderstorms (Uman and
60 Krider, 1989; Rosenfeld et al., 2008; Fan et al., 2018); and for investigating related atmospheric
61 chemistry, such as the formation of ozone and the primary oxidant in the troposphere, the
62 hydroxyl radical (Pickering et al., 2016; Brune et al., 2021).

63 The determination of whether a cloud will evolve into a thunderstorm is very difficult. The
64 occurrence of lightning activity in clouds is a complex process involving dynamics, microphysics
65 and electrical processes (e.g., Krehbiel et al., 1979; MacGorman and Rust, 1998; Carey and
66 Rutledge, 2000; Stolzenburg et al., 2001; Saunders, 2008; Zhang et al., 2009; Lang and Rutledge,
67 2011; Zhang et al., 2016; Stough and Carey, 2020; Lyu et al., 2023). Moreover, natural lightning
68 flashes are generally defined as intracloud lightning and cloud-to-ground lightning~~shows~~
69 ~~different types depends on different environments~~ (Uman and Krider, 1989; ~~Boggs et al., 2022~~);
70 ~~intracloud lightning, cloud-to-ground lightning, cloud-to-cloud and cloud-to-air discharges~~. Some
71 studies have indicated that the majority of the first lightning flashes are intracloud lightning,
72 which was concluded from the statistical results observed by polarimetric radar and lightning
73 location systems (e.g., Mattos et al., 2017; Zhao et al., 2021a). ~~And~~In addition, there is a
74 generally accepted electrification cause, especially for clarifying the first lightning flash
75 occurrence correctly: noninductive charging (NIC) of two ice particles of different sizes during
76 rebounding collisions in the presence of supercooled droplets, with the smaller ice particle being
77 the ice crystal and the larger ice particle being the graupel; aerosol provides the cloud
78 condensation nuclei and ice nuclei for hydrometeor formation, thus playing an important role in
79 cloud electrification (Takahashi, 1978; Latham, 1981; Saunders et al., 1991; MacGorman and
80 Rust, 1998; Carey and Rutledge, 2000; Rosenfeld et al., 2008; Zhang et al., 2009; Takahashi et
81 al., 2017, 2019; Qie et al., 2021; Lyu et al., 2023).

82 The NIC was proposed ~~based~~ on the basis of cold-chamber laboratory experiments

83 (Reynolds et al., 1957; Takahashi, 1978); subsequently, field observations demonstrated that
84 lightning production is critically linked to ice processes (i.e., graupel signatures) (Dye et al., 1986;
85 Takahashi et al., 1999; Carey and Rutledge, 2000; Basarab et al., 2015; Stolzenburg et al., 2015;
86 Mattos et al., 2016, 2017; Takahashi et al., 2017, 2019; Hayashi et al., 2021; Zhao et al., 2022).
87 Numerical simulation studies also support the NIC mechanism as the main contributor to charge
88 separation conducive to lightning flash triggering at timescales relevant to storm duration (e.g.,
89 Helsdon et al., 2001; Mansell et al., 2005; Barthe and Pinty, 2007). Therefore, graupel is a vital
90 precipitation particle for riming electrification mechanism.

91 Graupel is rimed precipitation ice. ~~However,~~But the mechanisms for graupel formation ~~will~~
92 vary with cloud types. One pathway to graupel that is very common in warm based clouds
93 worldwide is the development of rain drops in warm rain collision-coalescence processes (e.g.,
94 Brahams, 1986; Beard, 1992; Herzegh and Jameson, 1992; Bringi et al., 1997; Carey and
95 Rutledge, 2000), followed by lofting of the rain drop in the updraft ~~to the supercooled~~
96 temperature to subfreezing temperatures (which is frequently observed by polarimetric radar,
97 called the differential reflectivity (Z_{DR}) column), then by drop freezing and finally riming into
98 graupel or small hail. This coalescence-freezing mechanism is often the most important pathway
99 to the first graupel/hail, the first significant electrification and the first lightning flash in warm
100 based clouds (e.g., Brahams, 1986; Beard, 1992; Herzegh and Jameson, 1992; Bringi et al., 1997;
101 Smith et al., 1999; Carey and Rutledge, 2000; Stolzenburg et al., 2015; Mattos et al., 2017).
102 Another pathway to graupel or small hail production is initiated via the aggregation of ice
103 crystals into snow aggregates, followed by riming of the snow aggregate into graupel and
104 possibly even small hail as the rime density increases (Heymsfield, 1982; Li et al., 2018).

105 It should also be emphasized that the formation of graupel is closely related to not only ~~the~~
106 lightning activity but also the strength of ~~updraft~~updrafts in clouds, and the latent heat of freezing
107 enhances updrafts, promoting severe storm formation (Rosenfeld, 1999; Zhang et al., 2004;
108 Rosenfeld et al., 2008). More droplets freeze aloft and release more latent heat for nucleation,
109 thereby invigorating convective updrafts and producing lightning, and deep convective clouds
110 form (Rosenfeld, 1999; Zhang et al., 2004; Rosenfeld et al., 2008). Therefore, investigating the
111 ice microphysics associated with graupel is essential for understanding ~~the~~ thunderstorm

112 formation.

113 Polarimetric radar is a better observation system for tracking the specific location and
114 timing of a cloud and inferring the microphysical characteristics within clouds (e.g., Seliga and
115 Bringi, 1976; Zrníc and Ryzhkov, 1999; Kumjian, 2013; Hu et al., 2019; Huang et al., 2023).
116 Many studies (e.g., Laksen and Stansbury, 1974; Marshall and Radhakant, 1978; Dye et al., 1986;
117 Vincent et al., 2003; [Latham et al., 2007](#); Woodard et al., 2012; Mattos et al., 2016, 2017;
118 Hayashi et al., 2021; Zhao et al., 2022) have investigated the relationship between ice
119 microphysics and lightning activity, and provided methods ~~to predict~~[for predicting](#) the first
120 lightning flash occurrence based on the riming electrification mechanism; specifically, ~~the~~
121 graupel-related reflectivity at -10°C or colder is a commonly supported leading reflectivity
122 parameter ~~for~~[in](#) forecasting the first lightning flash (e.g., [Laksen and Stansbury, 1974](#); [Marshall](#)
123 [and Radhakant, 1978](#); [Vincent et al., 2003](#); [Woodard et al., 2012](#); [Hayashi et al., 2021](#)). However,
124 the performances of these methods vary with seasons, geography, or other atmospheric variables;
125 more directly, different ice microphysics within different clouds dominate. There is no doubt that
126 the graupel signatures inferred by polarimetric radar [are](#) universally present in convective clouds,
127 ~~while~~[whereas](#) some clouds involve no lightning (e.g., Woodard et al., 2012; Hayashi et al., 2021;
128 Cui et al., 2022; Zhao et al., 2022). Specifically, the graupel signature inferred by [the](#)
129 polarimetric radar needs to be partitioned into more details according to the radar parameters.
130 Therefore, we [conducted this study](#)~~hope~~ to better understand the ice microphysics associated with
131 graupel within thunderstorms ~~in this study~~.

132 We [accomplished](#) this goal by comparing the ice microphysics associated with graupel
133 between isolated thunderstorms and non-thunderstorms during the warm season over southern
134 China and quantifying differences ~~in~~[of](#) graupel magnitude and shape (implying the riming
135 efficiency) in radar parameters, instead of studying the evolution variation within the same
136 thunderstorm (the role of some polarimetric signatures would be covered in the same cloud
137 evolution). [Furthermore, we discussed the possible microphysics associated with the source](#)
138 [initiation and channel of the first lightning flash via 3D lightning mapping](#). ~~To the best of our~~
139 knowledge, no other study addressing this topic has been published ~~yet~~. In addition, we [explored](#)
140 the role of the coalescence-freezing mechanism in the production of lightning based on the

141 information provided by the Z_{DR} column, a narrow vertical extension of positive Z_{DR} values
142 above the 0°C isothermal height associated with updrafts and supercooled liquid water in deep
143 moist convective storms (e.g., Hall et al., 1980; Ryzhkov et al., 1994; Kumjian and Ryzhkov,
144 2008; Kumjian, 2013; Kumjian et al., 2014; Snyder et al., 2015; Zhao et al., 2020; Chen et al.,
145 2023). Isolated thunderstorms are common in southern China during the warm season (Mai and
146 Du, 2022). From the perspective of isolated storms in the warm season, the physical processes
147 within clouds ~~are will be~~ easier to explain, and the characteristics of graupel microphysics
148 ~~can could~~ be compared with those of that in cold-based clouds (~~results in~~ Li et al., 2018).

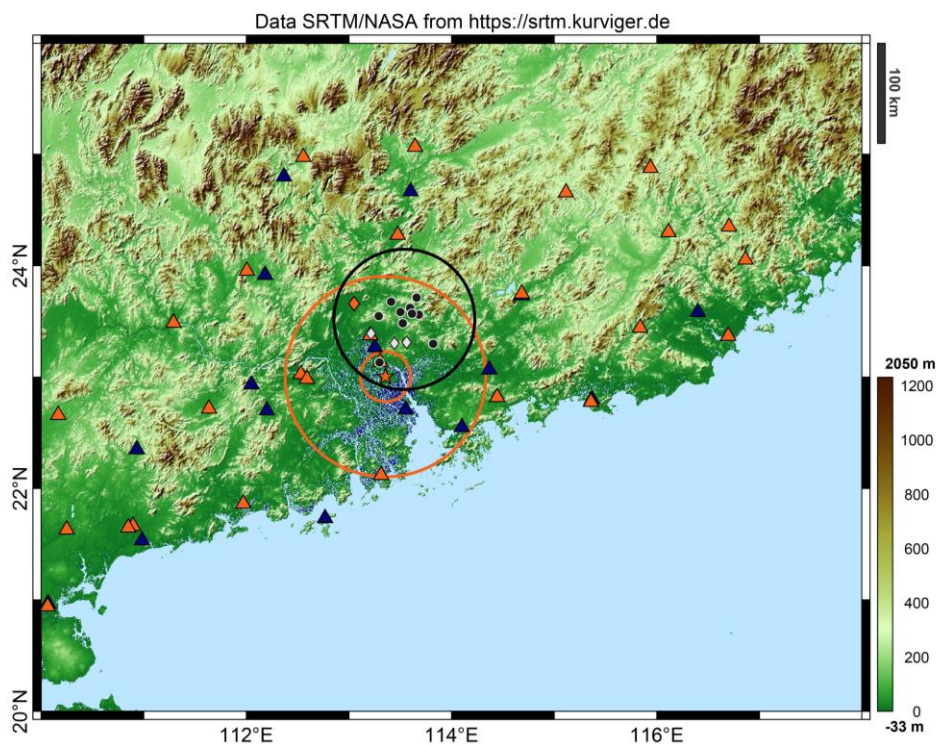
149 2. Materials and methods

150 ~~In this study, 57/39 isolated thunderstorm/non-thunderstorm cells that occurred over South~~
151 ~~China in the warm seasons (from late May to early September) of 2016 and 2017 were analysed;~~
152 ~~The~~ dataset used in this study was the same as that used in Zhao et al. (2021a, 2022). In Zhao et
153 al. (2021a), the dataset was first shown to the public, who obtained observations of 57 (39)
154 isolated thunderstorms (non-thunderstorms) that occurred over South China in the warm season
155 (from late May to early September) of 2016 and 2017 from the S-band polarimetric radar and
156 three independent lightning location systems. The role of turbulence characteristics in producing
157 the first lightning flashes was evaluated on the basis of the dataset, and the results indicated that
158 the eddy dissipation rate of non-thunderstorms was clearly lower than that of thunderstorms (Zhao
159 et al., 2021a). Moreover, the polarimetric radar parameters of the first radar echoes (the first radar
160 volume scan when clouds are detected by radar) were compared to determine the early difference
161 between thunderstorms and non-thunderstorms on the basis of this dataset (Zhao et al., 2022). The
162 greater echo intensity occurred in non-thunderstorms below the -10°C isotherm height, and the
163 cause for this feature and effect on subsequent cloud development were simply discussed by
164 integrating comprehensive observations (e.g., the ERA-Interim reanalysis data, surface aerosol
165 concentration, and graupel and rainwater contents derived from radar observations).

166 The error in the graupel content estimated in Zhao et al. (2022) is uncertain, and the
167 efficiency of the microphysical process (i.e., riming) associated with graupel is unknown; this
168 represents a gap in understanding regarding the role of graupel in the first lightning flash
169 occurrence based on field observations. Naturally, we aimed to identify a method to quantify

170 differences in graupel magnitude and riming efficiency in this study to minimize the error as much
171 as possible. The radar sample volume, which corresponds to graupel identification, was used to
172 indicate the graupel magnitude instead of the derived graupel content, as in Carey and Rutledge
173 (2000) and Zhao et al. (2022). The variety of Z_{DR} shapes was used to determine the riming
174 efficiency. Thus, the goal and method of this study were substantially different from those of the
175 two previous studies noted above, although they are based on the same dataset.

176 The Guangzhou ~~S-pol~~S-band polarimetric radar (GZ radar) provided the radar data as marked
177 by the orange star in Figure 1. The beam width of the ~~GZS-pol~~GZ radar was $\leq 1^\circ$, and a full radar
178 volume scan lasted 6 minutes; this consisted of nine elevation angles with a radial resolution of
179 250 m. A quality control procedure was carried out to remove ~~the~~ ground clutter, anomalous
180 propagation, and biological scatter, and the Z_{DR} offset of the raw data was corrected (Zhao et al.,
181 2022). The quality-controlled radar data were interpolated onto a Cartesian grid at a horizontal
182 resolution of 250 m and a vertical resolution of 500 m ~~from~~ over 0.5 to 20 km above the mean sea
183 level ~~using~~ via nearest neighbour and vertical linear interpolation.



184
185 **Figure 1. The locations of the detection systems and the analysed area. The orange star indicates**
186 **the Guangzhou S-band polarimetric radar (GZ radar); the orange circles represent distances from the**

187 GZ radar site of 25 and 100 km. The black dots indicate the 10 sensors of the Low-Frequency E-field
188 Detection array (LFEDA); the black circle indicates the distance from the centre of the LFEDA
189 network to 70 km. The blue triangles indicate the 16 sensors of the Earth Networks Lightning Location
190 System (ENLLS), and the orange triangles indicate the 27 sensors of the Guangdong Lightning
191 Location System (GDLLS). The white diamonds indicate the three ground sites of aerosol
192 concentration measurements. The orange diamond indicates the Qingyuan meteorological observatory.
193 The analysed area is restricted to the regions of overlapping coverage between the GZ radar radius of
194 25–100 km and the LFEDA station network centre radius of 70 km.

195 A hydrometeor identification method, which is based on the fuzzy logic algorithm, was
196 carried out to discriminate the graupel particles, as in Zhao et al. (2021b). The algorithm and
197 approximate ranges of the S-band values of each polarimetric variable essentially followed Park et
198 al. (2009) and Kumjian (2013), with an improvement in the parameters ~~of~~ the membership
199 functions of the fuzzy logic algorithm for the performance of the GZ radar-Guangzhou S-pol radar,
200 especially for dry/wet snow particles (Wu et al., 2018). In addition, temperature information was
201 ~~added as~~ one of ~~the~~ few factors added to the hydrometeor identification method because it
202 ~~can~~~~could~~ separate ~~the~~ liquid precipitation from ~~the~~ solid hydrometeors to avoid visible
203 identification errors (e.g., Bechini and Chandrasekar, 2015; Kouketsu et al., 2015; Zhao et al.,
204 2020).

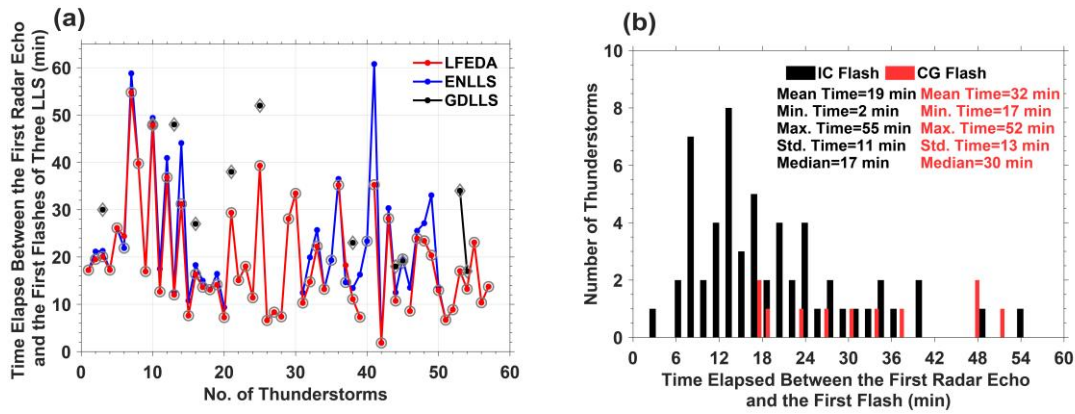
205 Three independent lightning location systems provided lightning observations. The
206 low-frequency E-field detection array (LFEDA, as marked by black dots in Figure 1) can detect
207 three-dimensional structures of intracloud lightning and/or cloud-to-ground lightning. The
208 detection efficiency and mean location error of LFEDA for triggered lightning were approximately
209 100% and 102 m, respectively (Shi et al., 2017; Fan et al., 2018). The Earth Networks Lightning
210 Location System (ENLLS, as marked by blue triangles in Figure 1) can detect two-dimensional
211 locations for intracloud lightning and/or cloud-to-ground lightning. The detection efficiency and
212 mean location error of ~~the~~ ENLLS for triggered lightning and the natural strike of tall structure
213 lightning were approximately 77% and 685 m, respectively (Zheng et al., 2017). The Guangdong
214 Lightning Location System (GDLLS, as marked by orange triangles in Figure 1) can locate
215 cloud-to-ground lightning. The detection efficiency and mean location error of the GDLLS for
216 triggered lightning and the natural strike of tall structure lightning were approximately 94% and
217 741 m, respectively (Chen et al., 2012).

218 ~~Three lightning location systems were used to more accurately detect the first lightning~~
219 ~~flashes within clouds.~~ The lightning flash was assigned to its corresponding cell by using the
220 boundary of the cell as a constraint every 6 minutes. The first lightning flash of a thunderstorm
221 was defined by its first detection from one of three lightning location systems. An isolated
222 non-thunderstorm cell was selected when no flash in the cell was detected by any of the three
223 lightning location systems. To ensure detection-data quality, the analysis area was restricted to the
224 regions of overlapping coverage between the ~~GZS-pol~~ radar radius of 25–100 km and the LFEDA
225 station network centre radius of 70 km (Figure 1), as in Zhao et al. (2021a, 2022). Any isolated
226 cell storm generated within the analysis area that moved completely outside the analysis area or
227 merged with other precipitation cells was excluded. The intersection of the 20 dBZ contours of the
228 two ~~intersecting~~~~intersected~~ cells is referred to as merging. For thunderstorms, we ensure that the
229 first lightning flash of the cell must occur before merging or when there is no merging. For storm
230 cell development, if no merging process occurs and the maximum reflectivity of this cell starts to
231 fade with a value of less than 30 dBZ later, the evolutionary process of a cell will mark the
232 cessation stage. Our objective ~~was~~~~is~~ to focus on isolated storm cells; therefore, if ~~the~~ merging
233 process occurs before the fading of the maximum reflectivity of this cell, the evolutionary process
234 of the cell will also signal the cessation stage.

235 In the dataset, six merging events occurred in non-thunderstorms, and the values of maximum
236 reflectivity for these non-thunderstorms did not increase after merging occurred. In addition, the
237 maximum reflectivity within any non-thunderstorm cell from initiation to cessation must exceed
238 45 dBZ to avoid the statistics of weak precipitation cells. Non-thunderstorms are characterized by
239 no flash occurrence from initiation to cessation. The sounding data were obtained from the
240 Qingyuan meteorological observatory, ~~as marked by the orange diamond in Figure 1~~, which also
241 provided the environmental temperature. Isolated thunderstorm/non-thunderstorm cells were
242 identified and tracked manually based on the observations from the ~~GZS-pol~~ radar and lightning
243 location systems. The average distances between these storms and the radar/sounding site were
244 approximately 70 and 56 km, respectively. More details related to these data and the selection
245 methods for isolated thunderstorm and non-thunderstorm cells are available in Zhao et al. (2021a,
246 2022).

247 In this study, the evolution cycle of a thunderstorm ~~consists of~~contains three stages: (i) the
248 first radar volume scanning in cases where the horizontal reflectivity (Z_H) \geq 5 dBZ is called the
249 first stage (hereafter referred to as the #1 stage), (ii) the intermediate radar volume scanning
250 between the first stage and the third stage is called the second stage (hereafter referred to as the #2
251 stage), and (iii) the radar volume scanning in cases where the first lightning flash occurs is called
252 the third stage (hereafter referred to as the #3 stage). Similarly, the evolution cycle of a
253 non-thunderstorm also contains three stages, but radar volume scanning in cases where the most
254 intense echo occurs is called the third stage; here, the most intense echo is used to indicate the
255 strongest convection development stage of non-thunderstorms for comparison with the first
256 lightning flash stage of thunderstorms. The average durations from the first stage to the third stage
257 for thunderstorms and non-thunderstorms ~~were~~are 19 and 24 minutes, respectively.

258 The majority of first lightning flash events (~98%) ~~were~~are considered ~~to be~~ intracloud
259 flashes (IC flashes), and only one ~~was~~is considered ~~to be~~ a cloud-to-ground flash (CG flash)
260 (Figure 2a). The majority of first lightning flashes (~91%) ~~was~~are determined by the LFEDA
261 ~~because of~~ ~~due to~~ its superior detection efficiency and accuracy for detecting lightning flashes in
262 this analysis area (Figure 2a). ~~The elapsed time between the first radar volume scan and the first~~
263 ~~IC or CG flash (indicated by the first IC or CG return stroke) is shown in Figure 2b. The results~~
264 ~~show that the average elapsed time between the first radar volume scan and the first IC flash was~~
265 ~~approximately 19 minutes, and the first CG flash was approximately 32 minutes (Figure 2b). A~~
266 ~~recent study (Mattos et al., 2017) also revealed that in ~98% of thunderstorms, an IC flash~~
267 ~~preceded the first CG flash, and the IC flashes occurred approximately 29 minutes after the first~~
268 ~~radar echo (any reflectivity value (any value above the local noise floor of the radar) at any height),~~
269 ~~CG flashes were most frequently delayed by approximately 36 minutes. The definition of the first~~
270 ~~radar echo may be the possible reason that the first flashes occurring after the first radar echo in~~
271 ~~Mattos et al. (2017) occurred later than those in our study.~~



272

273 **Figure 2. Lightning observations.** Elapsed time between the first radar volume scan and (a) the first
 274 flashes of three lightning location systems, LFEDA (red line), ENLLS (blue line), and GDLLS (black
 275 line), where the grey circles indicate the first IC flashes, the grey diamonds indicate the first CG flashes,
 276 and (b) the elapsed time between the first radar volume scan and the first flashes of thunderstorms, the
 277 first IC flashes (black columns), and the first CG flashes (red columns).

278 In addition, the average 1-hourly surface concentration observations of particulate matter
 279 (PM_{2.5/10}) were provided by three ground sites (Figure 1, white diamonds) within the analysed area.
 280 The PM_{2.5/10} concentration data suggest that the environment prior to these isolated thunderstorms
 281 or non-thunderstorms was clean and that the difference in the environmental aerosol concentration
 282 between thunderstorms and non-thunderstorms may be small (the mean values of PM_{2.5/10}
 283 concentrations prior to thunderstorms and non-thunderstorms were 22.9/42 $\mu\text{g m}^{-3}$ and 20.5/38.8
 284 $\mu\text{g m}^{-3}$, respectively).

285 3. Results

286 3.1 Morphology and intensity of the echoes in and/or before the first lightning flash 287 occurrence

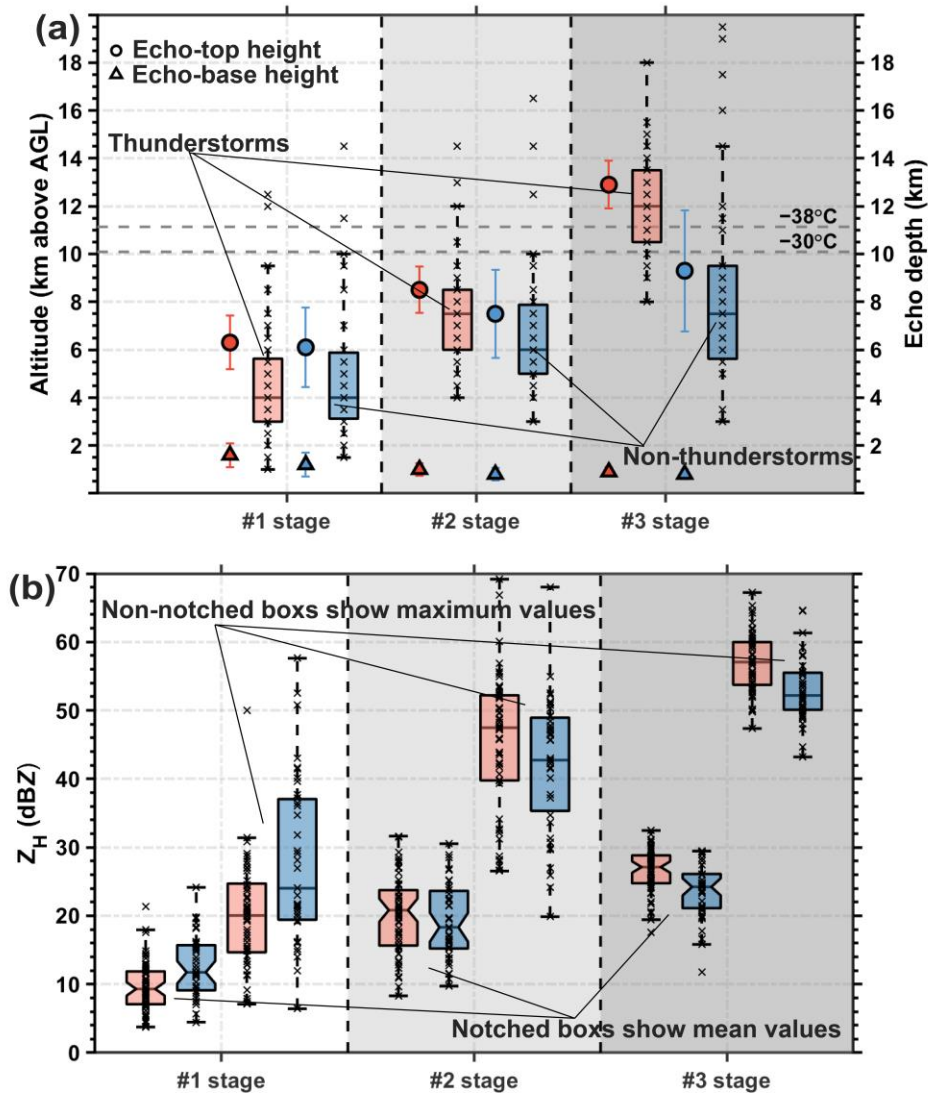
288 The ~~orange~~ scatters and ~~grey~~ triangles with error bars in Figure 31a ~~depict~~ describe the
 289 echo-top heights and echo-base heights of the 57 thunderstorms and 39 non-thunderstorms from
 290 the first stage to the third stage of cloud development ~~via~~ using the reflectivity threshold (0 dBZ),
 291 and the echo depths are shown in the box plots. The echo-top heights of thunderstorms ~~and~~
 292 non-thunderstorms increase as clouds develop. For the echo-top height data, approximately 95%
 293 of the thunderstorms exceeded the -30°C isotherm height, and 85% exceeded the -38°C isotherm
 294 height of the glaciated layer during the third stage of cloud development; however, only 26% and
 295 23% of ~~the~~ non-thunderstorms exceeded the -30°C and the -38°C isotherm heights, respectively,

296 during the third stage of cloud development. However, the echo-base heights mildly decreased
297 with the development of clouds; slight differences in the echo-base heights occurred between
298 thunderstorms and non-thunderstorms. ~~Deep convective clouds, indicated by thunderstorms, were~~
299 ~~formed when first lightning flashes occurred; approximately 84% of thunderstorms and only 23%~~
300 ~~of non-thunderstorms achieved an echo depth of 10 km.~~

301 When the first lightning flashes occurred, approximately 84% of the thunderstorms and only
302 23% of the non-thunderstorms achieved an echo depth of 10 km. Lightning is the product of the
303 severe storms, and scientists often equate storm intensity with lightning flashes (e.g., Zipser et al.,
304 2006; Fan et al., 2018), but defining convective intensity is not as easy as it may seem (Zipser et
305 al., 2006); this could provide supplementary quantitative evidence for assisting scientists in
306 equating storm intensity with lightning flashes and determining the cloud depth corresponding to
307 the first lightning flash occurrence.

308 Figure 3**4**b shows that the differences in the mean (maximum) values of the Z_H between the
309 thunderstorm and non-thunderstorm periods during each stage are slight; specifically, the median
310 differences in the mean values are -2, 2, and 3 dBZ, respectively. The median differences in the
311 maximum values are -4, 5, and 5 dBZ, respectively. Thunderstorms exhibit greater Z_H intensities
312 than non-thunderstorms do, except for those in the first stage of cloud development. The signature
313 of larger mean or maximum values of Z_H in non-thunderstorms during the first stage than in
314 thunderstorms has been discussed by Zhao et al. (2022), and this aspect is not the focus of this
315 study. The mean or maximum values of Z_H in thunderstorms increase and exceed those in
316 non-thunderstorms when the first lightning flashes occur; however, the box plots show that we
317 cannot effectively differentiate ~~the~~ thunderstorms from ~~the~~ non-thunderstorms with respect to the
318 Z_H intensity.

319



320

321 **Figure 31. Characteristics of radar echoes with cloud development.** (a) Echo-top heights of 0 dBZ
 322 and echo-base heights of 0 dBZ for 57 thunderstorm and 39 non-thunderstorm cells from the first stage
 323 to the third stage of cloud development are indicated by scatter points and triangles, respectively, with
 324 error bars. Error bars are computed as 95% confidence intervals. Box plots for the 57 thunderstorms
 325 (orange) and 39 non-thunderstorms (blue) for echo depths; all units are in km. The dashed grey lines
 326 indicate the -38°C and -30°C isotherm heights, respectively. (b) The mean (maximum) value of the
 327 Z_H in a thunderstorm or a non-thunderstorm during every stage is shown in notched box plots
 328 (non-notched box plots), with all units in the dBZ. The median values in the box plots are shown as
 329 black horizontal continuous lines. The temperature data were obtained from the sounding data of the
 330 Qingyuan meteorological observatory.

331 3.2 Variations in ~~the~~ graupel magnitude with cloud development

332 Graupel is a vital precipitation particle for the riming electrification mechanism, and its radar
 333 signature is not obscured by small ice particles. ~~In contrast, the radar signature of small ice~~

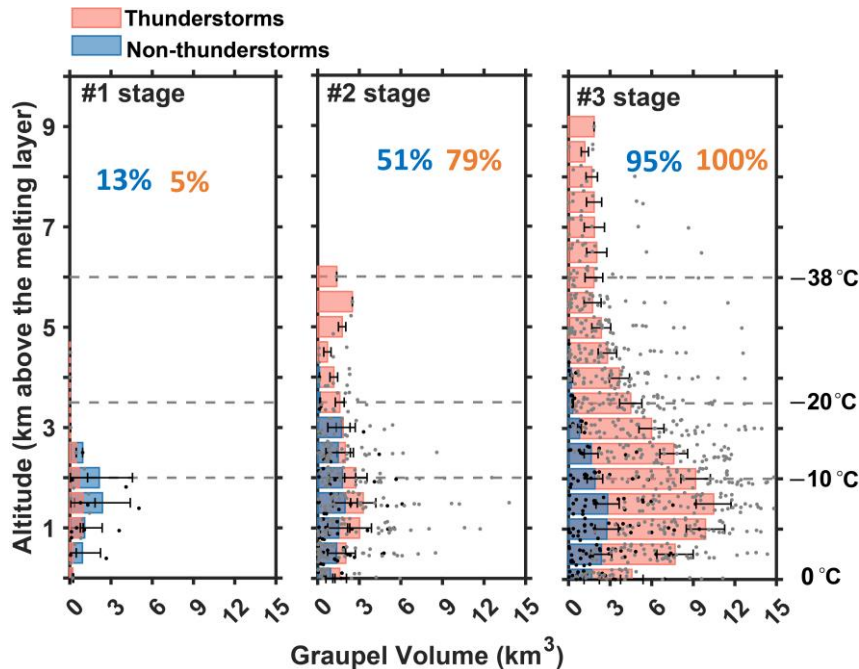
334 ~~particles (i.e., ice crystals) tends to be obscured by large ice particles (e.g., graupel).~~ Thus, to
335 investigate the microphysical characteristics related to the first lightning flash occurrence during
336 storms, we obtained inferred “graupel”, which was derived from the fuzzy-logic method based on
337 ~~the GZS-pol~~ radar (Park et al., 2009; Kumjian, 2013; Zhao et al., 2021b, 2022).

338 Each ~~bar~~ histrogram in Figure 42 indicates the mean value of the graupel volume in a height
339 layer (the definition of the height layer is a vertical resolution of 500 m over 0.5 to 20 km above
340 the mean sea level, 40 height layers in total) for 57 thunderstorms or 39 non-thunderstorms during
341 each stage of cloud development. Specifically, the volume is computed by accumulating the radar
342 sample grids; each radar sample grid is 0.03125 km^3 , $0.25 \text{ km} \times 0.25 \text{ km} \times 0.5 \text{ km}$. ~~(the volume is~~
343 ~~computed by the radar sample grid; each grid is 0.03125 km^3 , $0.25 \text{ km} \times 0.25 \text{ km} \times 0.5 \text{ km}$), which~~
344 ~~corresponds to the total graupel in total graupel on a height layer for 57 thunderstorms or 39~~
345 ~~non-thunderstorms during each stage of cloud development.~~

346 Graupel is rare in thunderstorms or non-thunderstorms during the first stage of cloud
347 development (e.g., Dye et al., 1986; Mattos et al., 2017), and only 5% (13%) of thunderstorms
348 (non-thunderstorms) show graupel signals (Figure 42). This finding is consistent with the results
349 of Lang and Rutledge (2011), who indicated that the existence of a 30 dBZ echo above the
350 freezing altitude is a necessary condition (in ~90% of cases) for lightning occurrence. This value is
351 well above the 5 dBZ threshold used in this study to detect the first stage of a storm and can
352 explain why graupel is rare in this stage. Moreover, in a modelling study of an isolated
353 thunderstorm, Barthe and Pinty (2007) reported a delay of ~20 minutes between the first
354 occurrence of graupel and the first lightning flash. In this case study, this delay was attributed to
355 the time for graupel and vapour-grown ice to locally gain charge through the NIC mechanism and
356 to the sedimentation of the different particles leading to macroscopic charge separation.

357 We proposed a mechanism for explaining the larger graupel volume in non-thunderstorms
358 during the first stage of cloud development: more warm precipitation growth in non-thunderstorms
359 due to cyclic drop growth resulting from coalescence under weaker updrafts may promote greater
360 drop formation (Kumjian et al., 2014; Mather et al., 1986; Stough et al., 2021). These larger drops
361 are lifted above the 0°C isothermal height and freeze to graupel-sized particles via a
362 coalescence-freezing mechanism (e.g., Bringi et al., 1997; Carey and Rutledge, 2000). With the

363 development of clouds, that proportion of ratio in thunderstorms (non-thunderstorms) that
 364 produced graupel reaches ~~is reached~~ 79% (51%) and 100% (95%) during the second and third
 365 stages of cloud development, respectively.



366

367 **Figure 42. Distribution of ~~the~~ graupel signals and volume with cloud development.** Histogram
 368 plots with error bars for the distribution of the graupel volume above the melting layer for thunderstorm
 369 and non-thunderstorm cells during each stage of cloud development. Each grey dot indicates the total
 370 graupel volume on a height layer (the definition of the height layer is a vertical resolution of 500 m
 371 over 0.5 to 20 km above the mean sea level, 40 height layers in total) of a thunderstorm; the black dots
 372 indicate non-thunderstorms (units in km^3). The mean graupel volume in a height layer for the 57
 373 thunderstorms is displayed as an orange histogram and a blue histogram shows the graupel volume for
 374 non-thunderstorm (in km^3). Error bars are computed as 95% confidence intervals. The numerical values
 375 in orange and blue are the percentages of thunderstorms and non-thunderstorms that show ~~the~~ graupel
 376 signals, respectively. The left column represents ~~is for~~ the first stage of cloud development, and the right
 377 and middle rows represent ~~are for~~ the third and second stages of cloud development, respectively. ~~In~~
 378 addition, the values are given by bilateral box plots. The -10°C , -20°C , and -38°C isotherm heights
 379 are displayed in the histogram plots.

380 The greatest difference in ~~the~~ graupel magnitude between thunderstorms and
 381 non-thunderstorms is found during the third stage of cloud development; the maximum difference
 382 in ~~the~~ graupel volume in a height layer reaches approximately 7.6 km^3 , and the height of the
 383 maximum difference is near the -10°C isotherm height. This information is consistent with the
 384 NIC electrification mechanism; namely, more graupel leads to more cloud electrification. In
 385 addition, more graupel corresponds to more latent heat being released for convection invigoration.

386 Interestingly, that the height corresponding to maximum difference of graupel volume is consistent
387 with the main negative charge layer in thunderstorms over Guangzhou (Liu et al., 2020). Thus, the
388 results suggested that the location of the negative charge layer may depend on the height of the
389 maximum graupel magnitude. ~~To note~~Notably, the graupel volume should be more accurately
390 phrased as the presence of graupel in this volume. These characteristics indicate that graupel
391 signals are universally present in thunderstorms and non-thunderstorms; and that the difference in
392 the magnitude of the graupel volume is the key for the first lightning flash occurrence.

393 **3.3 More microphysical information based on radar variables**

394 As the graupel volume increases from the first radar track to the occurrence of the first
395 lightning flash, the graupel volume in thunderstorms is clearly greater than that in
396 non-thunderstorms during the third stage of cloud development. However, the understanding of
397 the details of the increase in ~~the~~ graupel volume is limited (e.g., the variation in the maximum
398 dimension or number concentration and precursor signature). In addition, although the
399 coalescence-freezing mechanism dominating the formation of graupel within warm-season
400 thunderstorms is generally accepted (e.g., Brahams, 1986; Beard, 1992; Herzegh and Jameson,
401 1992; Bringi et al., 1997; Smith et al., 1999; Carey and Rutledge, 2000; Stolzenburg et al., 2015;
402 Mattos et al., 2017), more studies are needed to support this mechanism.

403 The Z_{DR} parameter could provide more information on ~~the~~ graupel (e.g., shape) (e.g., Mattos
404 et al., 2017; Li et al., 2018) and supercooled liquid water (e.g., Z_{DR} column) (e.g., Kumjian, 2013;
405 Kumjian et al., 2014). The variance in the shape of the graupel indicates the riming efficiency;
406 specifically, the heavily rimed ice particles approach a spherical shape (Kumjian, 2013; Li et al.,
407 2018). Although the shape cannot directly indicate the variation in the maximum dimension, the
408 speculated riming efficiency from the variation in the graupel shape could provide related
409 information on the maximum dimension of graupel particles; typically, a more spherical shape (a
410 decrease in Z_{DR}) and more riming result in a stronger Z_H corresponding to a larger maximum
411 dimension (Li et al., 2018). The supercooled liquid water indicated by positive Z_{DR} values above
412 the 0°C isothermal height is the precursor for freezing particles, followed by the embryo of
413 graupel particles (e.g., Carey and Rutledge, 2000). Thus, the existence and/or variance of the Z_{DR}
414 column before the occurrence of the first lightning flash could support the coalescence-freezing

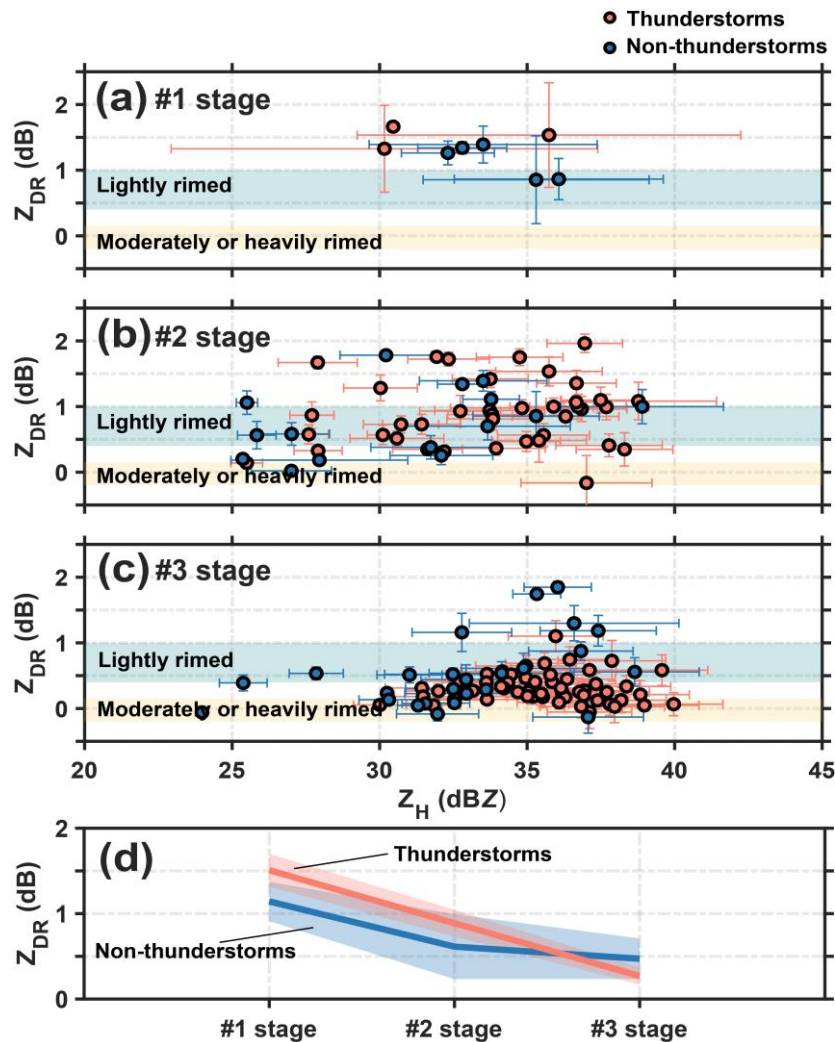
415 mechanism. Moreover, we can obtain the quantitative difference in the Z_{DR} between thunderstorms
416 and non-thunderstorms, especially for the occurrence of the first lightning flash.

417 *a. Differences in the shapes of ~~the~~ graupel particles between thunderstorms and*
418 *non-thunderstorms*

419 The mean values of Z_H and Z_{DR} corresponding to graupel particles (the radar sample grids are
420 identified as graupel) above the $\sim -3^\circ\text{C}$ isotherm height (avoiding melting effects) in
421 thunderstorms and non-thunderstorms during each stage of cloud development are displayed in
422 Figure 53. Each orange dot indicates the mean values of Z_H and Z_{DR} corresponding to graupel
423 above the $\sim -3^\circ\text{C}$ isotherm height in a thunderstorm; each blue dot indicates that in a
424 non-thunderstorm. ~~shows the average intensities of the Z_H and Z_{DR} with error bars corresponding~~
425 to the graupel particles above the $\sim -3^\circ\text{C}$ isotherm height (avoiding melting effects) in
426 thunderstorms and non-thunderstorms during each stage of cloud development. ~~Based on~~On the
427 basis of thesethe results, the average intensity of the Z_{DR} corresponding to the graupel particles
428 decreases with cloud development, which indicates that the graupel particles gradually approach a
429 spherical shape (Figure 53d). ~~The~~ The most remarkable indicator is that the graupel particles in the
430 majority of the thunderstorms have lower Z_{DR} values with a mean value of ~ 0.3 dB when the first
431 lightning flashes occur; however, this lower Z_{DR} value is not evident in non-thunderstorms, even
432 during the most intense echo stage of cloud development, with a ~~the~~ mean value of ~ 0.5 dB).
433 Moreover, the Z_{DR} values approach 0 dB, corresponding to stronger Z_H values when the average
434 intensity of the Z_H exceeds 35 dBZ. Thus, we speculated that heavily rimed graupel was present,
435 the size increased, and the shape tended to be spherical.

436 Li et al. (2018) presented a quantitative relationship between the riming and shape of snow
437 aggregates in only winter snowstorms; however, we examined the relationship in deep convection
438 or thunderstorms in the present study. In Li et al. (2018), particles with $Z_H > 15$ dBZ, $Z_{DR} > 0.4$ dB,
439 and above the $\sim -3^\circ\text{C}$ isotherm height are likely to be lightly rimed (rime mass fraction $\sim < 0.2$),
440 and particles with $Z_H > 15$ dBZ, $-0.2 < Z_{DR} < 0.15$ dB, and above the $\sim -3^\circ\text{C}$ isotherm height are
441 likely to be moderately or heavily rimed (rime mass fraction $\sim > 0.4$). The rime mass fraction is
442 defined as the ratio of the accreted ice mass to the total ice particle mass; more details on the rime
443 mass fraction can be found in Li et al. (2018). In Figures 53a, b, and c, the shaded area in blue

444 indicates the high possibility that graupel particles are lightly rimed; comparatively in contrast, the
 445 shaded area in yellow indicates that the graupel particles are moderately or heavily rimed, as in Li
 446 et al. (2018). The results from Li et al. (2018) are limited to only winter snowstorms; the
 447 mechanism for producing graupel in winter snowstorms is initiated via the aggregation of ice
 448 crystals into snow aggregates, followed by riming of the snow aggregate into graupel and possibly
 449 even small hail as the rime density increases (Heymsfield, 1982; Li et al., 2018). This process is
 450 different from ~~that~~ the coalescence-freezing mechanism in warm-season thunderstorms, but the
 451 final shape of the graupel particles when first lightning flashes occurred red in this study approached
 452 the shape of moderately or heavily rimed ice particles in Li et al. (2018).



453
 454 **Figure 53. Graupel shape in and/or before the first lightning flash occurrence.** Scatter plots with
 455 error bars for the mean values of Z_H and Z_{DR} corresponding to graupel particles above the $\sim -3^\circ\text{C}$
 456 isotherm height in thunderstorm (orange) and non-thunderstorm (blue) cells during each stage of cloud
 457 development. Error bars are computed as 95% confidence intervals. The inferred differences in the
 458 efficiency of the riming process are shown by the threshold values of Z_H and Z_{DR} ; the shaded area in

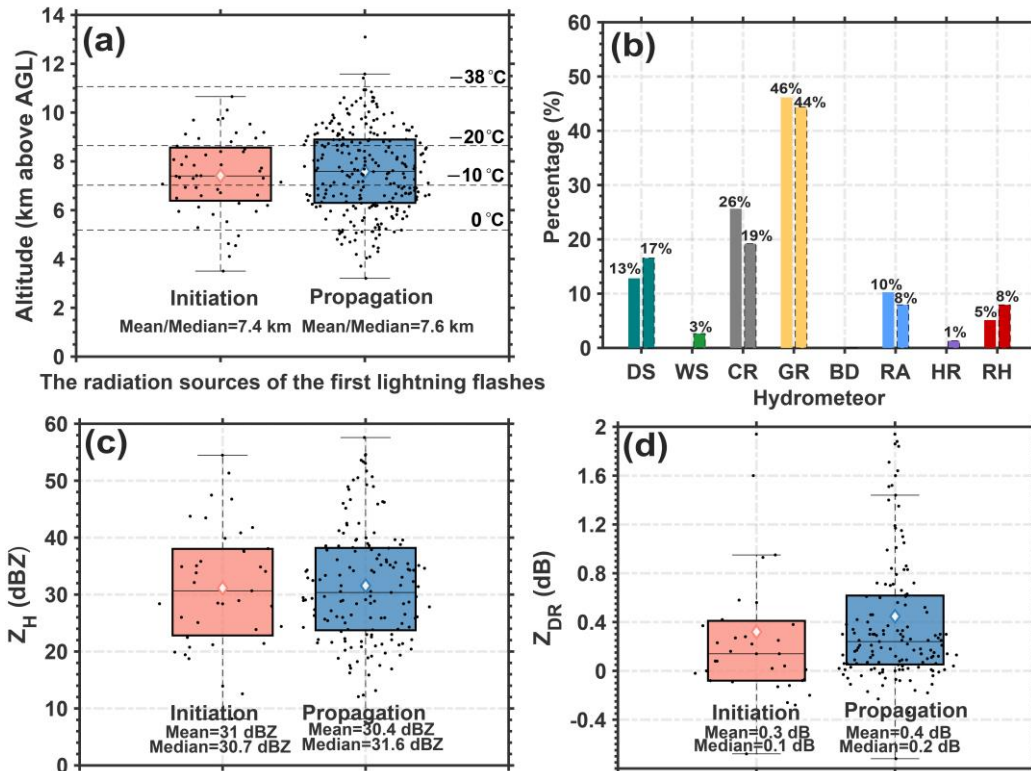
459 blue indicates the high possibility that graupel particles are lightly rimed, and comparatively, the
460 shaded area in yellow indicates that graupel particles are moderately or heavily rimed. (a) First stage, (b)
461 second stage, and (c) third stage of cloud development. In addition, the statistical mean values are
462 given in (d), and the orange (blue) line indicates the mean value of the Z_{DR} corresponding to the above
463 scatters in thunderstorms (non-thunderstorms) during each stage of cloud development. The shaded
464 area indicates the 95% confidence interval.

465 *b. ~~Signature of the Z_{DR} column~~ Observational characteristics associated with the source*
466 *initiation and channel of the first lightning flash*

467 The characteristics at positions with source initiation and channel characteristics of the first
468 lightning flash are shown in Figure 6, including the height distribution, associated hydrometeor
469 type, and values of Z_H and Z_{DR} . The heights of the initiation sources and propagation sources of
470 the first lightning flashes determined via LFEDA are concentrated at an approximate -10°C
471 isotherm height (Figure 6a), which is consistent with the results (i.e., the negative charge layer is
472 located at 6 to 8 km height in thunderstorms over Guangzhou) reported by Liu et al. (2020). The
473 hydrometeor types associated with the initiation and propagation sources are similar, and the
474 majority of these particles are graupel and ice crystals (Figure 6b), which is understandable on the
475 basis of the NIC electrification mechanism.

476 The median values of Z_H are near 31 dBZ, and the Z_{DR} values are near 0 dB (Figure 6c, d).
477 Furthermore, Figure 7 displays the frequency of initiation and propagation sources corresponding
478 to value intervals of Z_H (4 dBZ) and Z_{DR} (0.2 dB). The results indicate that the initiation sources of
479 the first lightning flashes likely correspond to 20~40 dBZ and $-0.2\sim 0.4$ dB (Figure 7a), and the
480 values are likely 16~44 dBZ and $-0.2\sim 0.8$ dB from propagation sources, respectively (Figure 7b).

481 These characteristics provide supplementary evidence that the main negative charge layer is
482 located at -10°C to -20°C isotherm height on Earth, as reported by Krehbiel (1986), and suggest
483 that are differences in particle shape and/or size between initiation sources and propagation
484 sources, although the differences are too subtle to quantify in this study.



485

486 **Figure 6. The characteristics at positions with source initiation and the channel of the first**
 487 **lightning flash.** (a) Height distribution of the locations at the initial sources (orange box) or
 488 propagation sources (blue box) of the first lightning flashes. The 0°C, -10°C, -20°C, and -38°C
 489 isotherm heights are displayed. (b) The histogram indicates the percentage of various hydrometeors of
 490 the locations at the initial sources or propagation sources (histogram with dashed line) of the first
 491 lightning flashes. The numerical value is the percentage of various hydrometeors, such as dry snow (DS,
 492 dark green), wet snow (WS, green), crystals (CR, grey), graupel (GR, yellow), big drops (BD),
 493 raindrops (RA, blue), heavy rain (HR, purple), and rain and hail mixtures (RH, red). Radar parameters
 494 of the locations at the initial sources (orange box) or propagation sources (blue box) of the first
 495 lightning flashes: (c) horizontal reflectivity (Z_H) and (d) differential reflectivity (Z_{DR}). Each black dot
 496 indicates an individual source. The diamonds indicate the mean values.

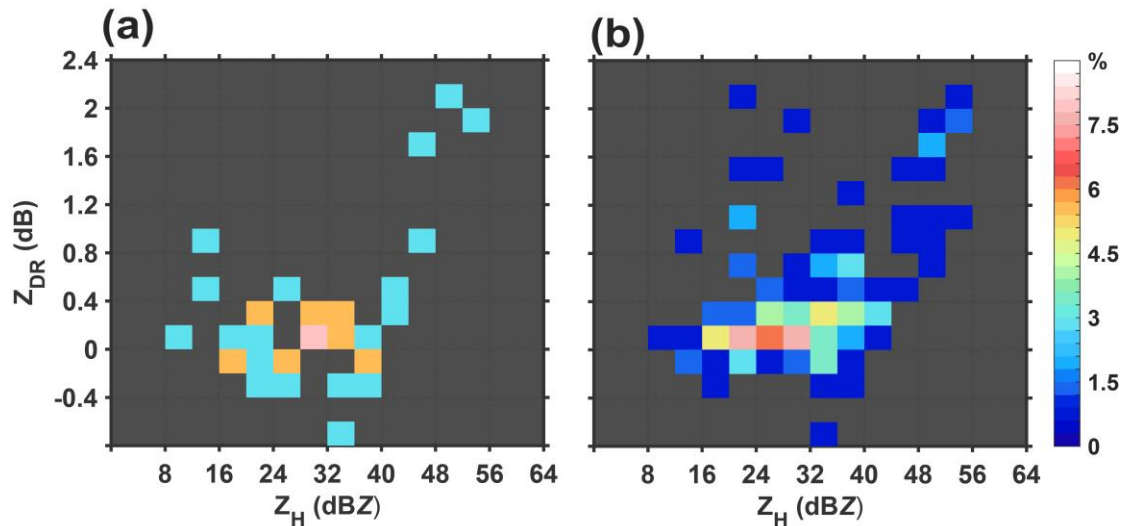


Figure 7. The frequency of radiation sources corresponding to the value intervals of Z_H and Z_{DR} .

(a) Initial sources. (b) Propagation sources.

c. Signature of the Z_{DR} column

Previous studies utilized Z_{DR} values ranging from 0.5–5 dB within the strong reflectivity range (35–50 dBZ) above the melting layer to describe the area of the Z_{DR} column (e.g., Illingworth et al., 1987; Tuttle et al., 1989; Ryzhkov et al., 1994; Scharfenberg et al., 2005; Woodard et al., 2012; Kumjian et al., 2014; Snyder et al., 2015; Zhao et al., 2020). Since the development of these clouds in this study occurred during the early stage of the full evolution cycle of thunderstorms, the size of the supercooled liquid water drop would not be large. Thus, we used Z_{DR} values of 0.5 dB within a reflectivity range of 30 dBZ above the melting layer to investigate the characteristics of the Z_{DR} column.

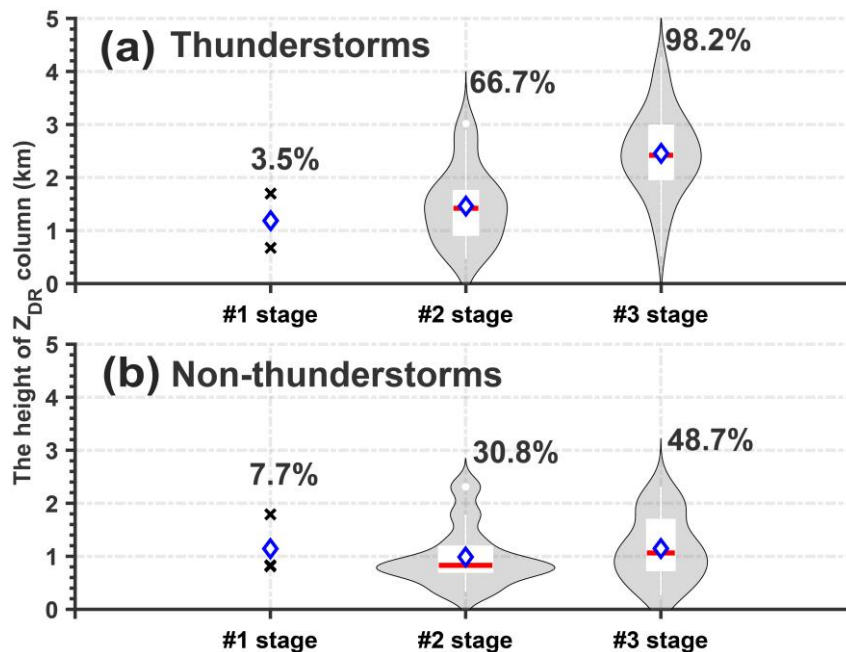
Figure 84 shows the height of the Z_{DR} column within thunderstorms or non-thunderstorms during each stage of cloud development. The computation of the Z_{DR} column height is similar to that in Snyder et al. (2015), and this height is the vertically continuous maximum depth of the Z_{DR} column. The signature of the Z_{DR} column clearly coincides with the development of clouds (Figure 84). Most thunderstorms (98.2%) displayed a deep Z_{DR} column with a mean depth of the Z_{DR} column of ~2.5 km when the first lightning flash occurred; however, only 48.7% of non-thunderstorms corresponded to a shallow Z_{DR} column with a mean value of ~1.1 km (Figure 84a, b). Moreover, 66.7% of the thunderstorms presented a deeper Z_{DR} column with a mean value of ~1.5 km during the second stage of cloud development, and 30.8% of the

518 non-thunderstorms ~~presented~~~~showed~~ a shallower Z_{DR} column with a mean value of ~ 0.99 km
 519 during the second stage of cloud development (Figure 84a, b).

520 The results indicate that strong relationship between the Z_{DR} column and the occurrence of
 521 the first lightning flash is persistent. A deeper Z_{DR} column suggests a greater graupel volume.

522 However, the occurrence frequency of the Z_{DR} column for non-thunderstorms is slightly greater
 523 than that for thunderstorms during the first stage of cloud development (Figure 84a, b). ~~However,~~

524 ~~this~~This phenomenon may be related to the results ~~off~~~~from~~ Zhao et al. (2022); specifically, the Z_{DR}
 525 values below the -10°C isotherm height of non-thunderstorms were greater than those of
 526 thunderstorms within the first radar echo.



528
 529 **Figure 84. Z_{DR} column information in and/or before the first lightning flash occurrence.** Violin
 530 plots of the Z_{DR} column depth of thunderstorm or non-thunderstorm cells during each stage of ~~the~~ cloud
 531 development, showing the average (blue diamond), interquartile range (rectangle), 10th and 90th
 532 percentiles (whiskers), and kernel density estimation (gr~~a~~ey shading). (a) Thunderstorms. (b)
 533 Non-thunderstorms. The numerical value is the percentage of thunderstorms that show the Z_{DR} column
 534 signature.

535 4. Summary

536 In this study, ~~a~~~~the~~ combination of a lightning location system and dual-polarization radar
 537 measurements was employed to study the ice microphysics of isolated thunderstorms and

538 non-thunderstorms in southern China during ~~the~~ warm season. From ~~the~~ unique perspective of
539 comparing ~~the~~ radar signatures and inferred graupel information between ~~the~~ isolated
540 thunderstorm and non-thunderstorm cells during each stage of cloud development, ~~the~~ lightning
541 generation in clouds was found to be ~~a~~ good indicator of the formation of deep convective clouds.
542 The echo intensities, echo-top heights and echo depths were greater in clouds when the first
543 lightning flash occurred, which indicated more severe updrafts in thunderstorms than in
544 non-thunderstorms. Moreover, a greater graupel volume ~~was~~ clearly observed in clouds when
545 the first lightning flash occurred, and the maximum difference in graupel volume in the height
546 layer between thunderstorms and non-thunderstorms reached approximately 7.6 km^3 ,
547 corresponding to an approximate -10°C isotherm height.

548 The variation in the average Z_{DR} intensity corresponding to the graupel particles above the
549 $\sim -3^\circ\text{C}$ isotherm height during the three stages of cloud development indicated that graupel
550 particles were more spherical (the mean Z_{DR} value was $\sim 0.3 \text{ dB}$) and were more likely to generate
551 lightning. The Z_{DR} values approached 0 dB , corresponding to stronger Z_{H} values; the average
552 intensity of the Z_{H} exceeded 35 dBZ . When the first lightning flashes occurred in clouds, a
553 decrease in the Z_{DR} value and an increase in the Z_{H} value of graupel were observed; these results
554 indicate that heavily rimed ice particles were present, and ~~that~~ the shape of these particles was
555 similar to that of moderately or heavily rimed ice particles within winter snowstorms.

556 Furthermore, observational characteristics associated with the source initiation and channel of
557 the first lightning flash were investigated. The results revealed that these sources were
558 concentrated at an isotherm height of approximately -10°C and mainly corresponded to graupel
559 and ice crystals. The median values of Z_{H} or Z_{DR} at the positions of source initiation and the
560 channel of the first lightning flashes were nearly 31 dBZ or 0 dB . In addition, we suggest that the
561 differences in particle shape and/or size between the initiation sources and propagation sources of
562 the first lightning flashes persist.

563 Moreover, the results indicated ~~that the highly related~~ a strong relationship between the Z_{DR}
564 column and the occurrence of the first lightning flash ~~was present~~; 98.2% of the clouds were
565 equipped with a Z_{DR} column with a mean depth of $\sim 2.5 \text{ km}$ when the first lightning flash occurred.
566 In addition, a deeper Z_{DR} column corresponded to a greater graupel volume. Thus, the

567 coalescence-freezing mechanism dominated the formation of graupel within warm-season isolated
 568 thunderstorms over southern China, and the results were consistent with those of previous studies
 569 (e.g., Brahams, 1986; Beard, 1992; Herzegh and Jameson, 1992; Bringi et al., 1997; Smith et al.,
 570 1999; Carey and Rutledge, 2000; Stolzenburg et al., 2015; Mattos et al., 2017); but increased ~~ing~~
 571 the knowledge of the~~about~~ quantified characteristics of the Z_{DR} column for the first lightning flash
 572 occurrence in warm-season isolated thunderstorms ~~based on~~ the basis of relatively large sample
 573 statistics (Table 1 shows details of cases in related investigations for isolated thunderstorms).

References	Number of cases (thunderstorms)	Number of cases (non-thunderstorms)
Workman and Reynolds, 1949	12	×
Reynolds and Brook, 1956	5	×
Goodman et al., 1988	1	×
Ramachandran et al., 1996	2	×
Jameson et al., 1996	3	×
Woodard et al., 2012	31	19
Stolzenburg et al., 2015	3	×
Mattos et al., 2017	46	×

574 Table 1. Details of the cases in the references.

575 However, our results were obtained by comparing the characteristics of the polarimetric
 576 parameters according to the graupel particles inferred via~~by~~ a hydrometeor identification method.
 577 The inferred graupel volume was an indication that graupel could be present among other
 578 hydrometeors in that volume. From the perspective of radar, the dominant particle in this volume
 579 was graupel. Fortunately, we focused on comparing the graupel volume between ~~the~~
 580 thunderstorms and non-thunderstorms; therefore, we believe that the errors in this volume
 581 resulting from other secondary hydrometeors could be neutralized by ~~the~~ comparisons with the
 582 same detected data and methods.

583 In addition, unlike previous similar studies (e.g., Mattos et al., 2016, 2017), we studied the
 584 microphysical differences between isolated thunderstorms and non-thunderstorms during the
 585 warm season over southern China on the basis of polarimetric radar and lightning mapping array
 586 instead of studying the evolution variation within the same thunderstorm (Mattos et al., 2017) or
 587 studying the differences between storm vertical profiles in three-dimensional Cartesian boxes with

588 lightning and without lightning (Mattos et al., 2016).

589 ~~In addition, although~~ Although the results from this study could provide a possible index or
590 method based on polarimetric radar for warning of the first lightning flash occurrence within ~~the~~
591 warm-season cell storms, understanding the microphysical characteristics and applying that in the
592 numerical simulations would be the optimal method for providing ~~to provide~~ lightning flash
593 warnings in the future.

594

595

596 **Acknowledgements**

597 The authors acknowledge the Guangzhou Institute of Tropical and Marine Meteorology for
598 collecting and archiving the radar, the surface, and the lightning observations. And authors also
599 acknowledge the State Key Laboratory of Severe Weather, Chinese Academy of Meteorological
600 Sciences & Laboratory of Lightning Physics and Protection Engineering for three-dimensional
601 lightning location data. This research has been supported by the National Natural Science
602 Foundation of China (grants 42175090, 42305079, 42305087), the China Postdoctoral Science
603 Foundation (grant 2023M730619), the Scientific Research Fund of Chengdu University of
604 Information Technology (grants KYTZ202213, KYQN202301, KYQN202307), the Scientific
605 Research Fund of CAMS State Key Laboratory of Severe Weather (2021LASW-B02), and Basic
606 Research Fund of CAMS (451490, 2023Z008).

607

608 **Open Research**

609 The sounding data is available at <http://weather.uwyo.edu/upperair/sounding.html>. The data in this
610 study can be obtained from Figshare (Zhao, 2024).

611

612

613 **References**

614 Barthe, C., and Pinty, J.-P.: Simulation of electrified storms with comparison of the charge

615 [structure and lightning efficiency, *Journal of Geophysical Research*, 112, D19204,](#)
616 [doi:10.1029/2006JD008241, 2007.](#)

617 Basarab, B. M., Rutledge, S. A., and Fuchs, B. R.: An improved lightning flash rate
618 parameterization developed from Colorado DC3 thunderstorm data for use in cloud-resolving
619 chemical transport models, *Journal of Geophysical Research: Atmospheres*, 120, 9481–9499,
620 doi:10.1002/2015JD023470, 2015.

621 Beard, K. V.: Ice initiation in warm-base convective clouds: An assessment of microphysical
622 mechanisms, *Atmospheric Research*, 28, 125–152,
623 [https://doi.org/10.1016/0169-8095\(92\)90024-5](https://doi.org/10.1016/0169-8095(92)90024-5), 1992.

624 Bechini, R., and Chandrasekar, V.: A Semisupervised Robust Hydrometeor Classification Method
625 for Dual-Polarization Radar Applications, *Journal of Atmospheric and Oceanic Technology*,
626 32, 22–47, <https://doi.org/10.1175/JTECH-D-14-00097.1>, 2015.

627 ~~Boggs, L. D., Mach, D., Bruning, E., Liu, N., van der Velde, O. A., Montanyá, J., Cummer, S.,~~
628 ~~Palivec, K., Chmielewski, V., MacGorman, D., and Peterson, M.: Upward propagation of~~
629 ~~gigantic jets revealed by 3D radio and optical mapping, *Science Advances*, 8, eabl8731, doi:~~
630 ~~10.1126/sciadv.abl8731, 2022.~~

631 Braham, R. R. Jr.: The cloud physics of weather modification. Part 1: Scientific basis, *WMO*
632 *Bulletin*, 35, 215–221, 1986.

633 Bringi, V. N., Knupp, K., Detwiler, A., Liu, L., Caylor, I. J., and Black, R. A.: Evolution of a
634 Florida Thunderstorm during the Convection and Precipitation/Electrification Experiment:
635 The Case of 9 August 1991, *Monthly Weather Review*, 125, 2131–2160, doi:
636 [https://doi.org/10.1175/1520-0493\(1997\)125<2131:EOAFTD>2.0.CO;2](https://doi.org/10.1175/1520-0493(1997)125<2131:EOAFTD>2.0.CO;2), 1997.

637 Brune, W. H., McFarland, P. J., Bruning, E., Waugh, S., MacGorman, D., Miller, D. O., Jenkins, J.
638 M., Ren, X., Mao, J., and Peischl, J.: Extreme oxidant amounts produced by lightning in
639 storm clouds, *Science*, 372, 711–715, doi: 10.1126/science.abg0492, 2021.

640 Carey, L. D., and Rutledge, S. A.: The Relationship between precipitation and lightning in tropical
641 island convection: A C-Band polarimetric radar study, *Monthly Weather Review*, 128,
642 2687–2710, [https://doi.org/10.1175/1520-0493\(2000\)128<2687:TRBPAL>2.0.CO;2](https://doi.org/10.1175/1520-0493(2000)128<2687:TRBPAL>2.0.CO;2), 2000.

643 Chen, G., Zhao, K., Wen, L., Yang, J., Zheng, Y., Xu, F., Lyu, F., Sun, K., and Sun, L.: Linking
644 ice-phase microphysics to raindrop characteristics in deep convection: A warm-sector

645 extreme rainfall case study in Eastern China, *Earth and Space Science*, 10, e2022EA002697,
646 <https://doi.org/10.1029/2022EA002697>, 2023.

647 Chen, L., Zhang, Y. J., Lyu, W., Zheng, D., Zhang, Y., Chen, S., and Huang, Z.: Performance
648 evaluation for a lightning location system based on observations of artificially triggered
649 lightning and natural lightning flashes, *Journal of Atmospheric and Oceanic Technology*, 29,
650 1835–1844, <https://doi.org/10.1175/JTECH-D-12-00028.1>, 2012.

651 Cui, Y., Zheng, D., Zhang, Y. J., Ruan, Z., Li, F., Yao, W., Meng, Q., and Zhao, C.: Association of
652 lightning occurrence with precipitation cloud column structure at a fixed position,
653 *Atmospheric Research*, 267, 105989, <https://doi.org/10.1016/j.atmosres.2021.105989>, 2022.

654 Dye, J. E., Jones, J. J., Winn, W. P., Cerni, T. A., Gardiner, B., Lamb, D., Pitter, R. L., Hallett, J.,
655 and Saunders, C. P. R.: Early electrification and precipitation development in a small, isolated
656 Montana cumulonimbus, *Journal of Geophysical Research: Atmospheres*, 91, 1231–1247,
657 <https://doi.org/10.1029/JD091iD01p01231>, 1986.

658 Fan, J. W., Rosenfeld, D., Zhang, Y., Giangrande, S. E., Li, Z., Machado, L. A. T., Martin, S. T.,
659 Yang, Y., Wang, J., Artaxo, P., Barbosa, H. M. J., Braga, R. C., Comstock, J. M., Feng, Z.,
660 Gao, W., Gomes, H. B., Mei, F., Pöhlker, C., Pöhlker, M. L., Pöschl, U., and de Souza, R. A.
661 F.: Substantial convection and precipitation enhancements by ultrafine aerosol particles,
662 *Science*, 359, 411–418, DOI: 10.1126/science.aan8461, 2018.

663 Fan, X., Zhang, Y. J., Zheng, D., Zhang, Y., Lyu, W., Liu, H., and Xu, L.: A new method of
664 three-dimensional location for low-frequency electric field detection array, *Journal of*
665 *Geophysical Research: Atmospheres*, 123, 8792–8812,
666 <https://doi.org/10.1029/2017JD028249>, 2018.

667 Goodman, S. J., Buechler, D. E., Wright, P. D., and Rust, W. D.: Lightning and precipitation
668 history of a microburst-producing storm, *Geophysical Research Letters*, 15, 1185–1188,
669 <https://doi.org/10.1029/GL015i011p01185>, 1988.

670 Hall, M. P. M., Cherry, S. M., Goddard, J. W. F., and Kennedy, G. R.: Rain drop sizes and rainfall
671 rate measured by dual-polarization radar, *Nature*, 285, 195–198,
672 <https://doi.org/10.1038/285195a0>, 1980.

673 Hayashi, S., Umehara, A., Nagumo, N., and Ushio, T.: The relationship between lightning flash
674 rate and ice-related volume derived from dual-polarization radar, *Atmospheric Research*, 248,

675 105166, <https://doi.org/10.1016/j.atmosres.2020.105166>, 2021.

676 [Helsdon Jr., J. H., Wojcik, W. A. and Farley, R. D.: An examination of thunderstorm-charging](#)
677 [mechanisms using a two-dimensional storm electrification model, *Journal of Geophysical*](#)
678 [Research: Atmospheres, 106\(D1\), 1165–1192, doi:10.1029/2000JD900532, 2001.](#)

679 Herzegh, P. H., and Jameson, A. R.: Observing Precipitation through Dual-Polarization Radar
680 Measurements, *Bulletin of the American Meteorological Society*, 73, 1365–1376,
681 [https://doi.org/10.1175/1520-0477\(1992\)073<1365:OPTDPR>2.0.CO;2](https://doi.org/10.1175/1520-0477(1992)073<1365:OPTDPR>2.0.CO;2), 1992.

682 Heymsfield, A. J.: A Comparative Study of the Rates of Development of Potential Graupel and
683 Hail Embryos in High Plains Storms, *Journal of the Atmospheric Sciences*, 39, 2867–2897,
684 [https://doi.org/10.1175/1520-0469\(1982\)039<2867:ACSOTR>2.0.CO;2](https://doi.org/10.1175/1520-0469(1982)039<2867:ACSOTR>2.0.CO;2), 1982.

685 Huang, H., Zhao, K., Chan, J. C. L., and Hu, D.: Microphysical Characteristics of
686 Extreme-Rainfall Convection over the Pearl River Delta Region, South China from
687 Polarimetric Radar Data during the Pre-summer Rainy Season, *Advances in Atmospheric*
688 *Sciences*, 40, 874–886, <https://doi.org/10.1007/s00376-022-1319-8>, 2023.

689 Hu, J., Rosenfeld, D., Ryzhkov, A., Zrníc, D., Williams, E., Zhang, P., Snyder, J. C., Zhang, R.,
690 and Weitz, R.: Polarimetric radar convective cell tracking reveals large sensitivity of cloud
691 precipitation and electrification properties to CCN, *Journal of Geophysical Research:*
692 *Atmospheres*, 124, 12194–12205, <https://doi.org/10.1029/2019JD030857>, 2019.

693 Illingworth, A. J., Goddard, J. W. F., and Cherry, S. M.: Polarization radar studies of precipitation
694 development in convective storms, *Quarterly Journal of the Royal Meteorological Society*,
695 113, 469–489, <https://doi.org/10.1002/qj.49711347604>, 1987.

696 Jameson, A. R., Murphy, M. J. and Krider, E. P.: Multiple-parameter radar observations of
697 isolated Florida thunderstorms during the onset of electrification, *Journal of Applied*
698 *Meteorology and Climatology*, 35, 343–354,
699 [https://doi.org/10.1175/1520-0450\(1996\)035<0343:MPROOI>2.0.CO;2](https://doi.org/10.1175/1520-0450(1996)035<0343:MPROOI>2.0.CO;2), 1996.

700 Kouketsu, T., Uyeda, H., Ohigashi, T., Oue, M., Takeuchi, H., Shinoda, T., Tsuboki, K., Kubo, M.,
701 and Muramoto, K.: A Hydrometeor Classification Method for X-Band Polarimetric Radar:
702 Construction and Validation Focusing on Solid Hydrometeors under Moist Environments,
703 *Journal of Atmospheric and Oceanic Technology*, 32, 2052–2074,
704 <https://doi.org/10.1175/JTECH-D-14-00124.1>, 2015.

705 Krehbiel, P. R., Brook, M., and McCrory, R. A.: An Analysis of the Charge Structure of Lightning
706 Discharges to Ground, *Journal of Geophysical Research*, 84, 2432–2456,
707 doi:10.1029/JC084iC05p02432, 1979.

708 Kumjian, M. R.: Principles and applications of dual-polarization weather radar. Part I: Description
709 of the polarimetric radar variables, *Journal of Operational Meteorology*, 1, 226–242,
710 doi:10.15191/nwajom.2013.0119, 2013.

711 Kumjian, M. R., Khain, A. P., Benmoshe, N., Ilotoviz, E., Ryzhkov, A. V., and Phillips, V. T. J.:
712 The anatomy and physics of ZDR columns: Investigating a polarimetric radar signature with
713 a spectral bin microphysical model, *Journal of Applied Meteorology and Climatology*, 53,
714 1820–1843, <https://doi.org/10.1175/JAMC-D-13-0354.1>, 2014.

715 Kumjian, M. R., and Ryzhkov, A. V.: Polarimetric signatures in supercell thunderstorms, *Journal*
716 *of Applied Meteorology and Climatology*, 47, 1940–1961,
717 <https://doi.org/10.1175/2007JAMC1874.1>, 2008.

718 Laksen, H. R., and Stansbury, E. J.: Association of lightning flashes with precipitation cores
719 extending to height 7 km, *Journal of Atmospheric and Terrestrial Physics*, 36, 1547–1548,
720 [https://doi.org/10.1016/0021-9169\(74\)90232-3](https://doi.org/10.1016/0021-9169(74)90232-3), 1974.

721 Lang, T. J., and Rutledge, S. A.: A Framework for the Statistical Analysis of Large Radar and
722 Lightning Datasets: Results from STEPS 2000, *Monthly Weather Review*, 139, 2536–2551,
723 <https://doi.org/10.1175/MWR-D-10-05000.1>, 2011.

724 Latham, J.: The electrification of thunderstorms, *Quarterly Journal of the Royal Meteorological*
725 *Society*, 107, 277–298, <https://doi.org/10.1002/qj.49710745202>, 1981.

726 [Latham, J., Petersen, W. A., Deierling, W. and Christian, H. J.: Field identification of a unique](#)
727 [globally dominant mechanism of thunderstorm electrification, *Quarterly Journal of the Royal*](#)
728 [*Meteorological Society*, 133, 1453–1457, <https://doi.org/10.1002/qj.133>, 2007.](#)

729 Li, H., Moisseev, D., and von Lerber, A.: How does riming affect dual-polarization radar
730 observations and snowflake shape? *Journal of Geophysical Research: Atmospheres*, 123,
731 6070–6081, <https://doi.org/10.1029/2017JD028186>, 2018.

732 [Liu, Z., Zheng, D., Guo, F., Zhang, Y., Zhang, Y. J., Wu, C., Chen, H., Han, S.: Lightning activity](#)
733 [and its associations with cloud structures in a rainstorm dominated by warm precipitation,](#)
734 [*Atmospheric Research*, 246, 105120, <https://doi.org/10.1016/j.atmosres.2020.105120>, 2020.](#)

735 Lyu, W., Zheng, D., Zhang, Y., Yao, W., Jiang, R., Yuan, S., Liu, D., Lyu, F., Zhu, B., Lu, G.,
736 Zhang, Q., Tan, Y., Wang, X., Liu, Y., Chen, S., Chen, L., Li, Q., and Zhang, Y. J.: A Review
737 of Atmospheric Electricity Research in China from 2019 to 2022, *Advances in Atmospheric*
738 *Sciences*, 40, 1457–1484, <https://doi.org/10.1007/s00376-023-2280-x>, 2023.

739 MacGorman, D. R., and Rust, W. D.: The electrical nature of storms, *Oxford University Press*, 422
740 pp., 1998.

741 Mai, C., and Du, Y.: Mesoscale moisture transport in determining the location of daytime
742 convection initiations clustered in time and space over southern China, *Journal of*
743 *Geophysical Research: Atmospheres*, 127, e2021JD036098,
744 <https://doi.org/10.1029/2021JD036098>, 2022.

745 Mansell, E. R., MacGorman, D. R., Ziegler, C. L., and Straka, J. M.: Charge structure and
746 lightning sensitivity in a simulated multicell thunderstorm, *Journal of Geophysical Research:*
747 *Atmospheres*, 110, D12101, doi:10.1029/2004JD005287, 2005.

748 Marshall, J. S., and Radhakant, S.: Radar Precipitation Maps as Lightning Indicators, *Journal of*
749 *Applied Meteorology and Climatology*, 17, 206–212,
750 [https://doi.org/10.1175/1520-0450\(1978\)017<0206:RPMALI>2.0.CO;2](https://doi.org/10.1175/1520-0450(1978)017<0206:RPMALI>2.0.CO;2), 1978.

751 Mather, G. K., Morrison, B. J., and Morgan, G. M.: A Preliminary Assessment of the Importance
752 of Coalescence in Convective Clouds of the Eastern Transvaal, *Journal of Applied*
753 *Meteorology and Climatology*, 25, 1780–1784,
754 [https://doi.org/10.1175/1520-0450\(1986\)025<1780:APAOTI>2.0.CO;2](https://doi.org/10.1175/1520-0450(1986)025<1780:APAOTI>2.0.CO;2), 1986.

755 Mattos, E. V., Machado, L. A. T., Williams, E. R., and Albrecht, R. I.: Polarimetric radar
756 characteristics of storms with and without lightning activity, *Journal of Geophysical*
757 *Research: Atmospheres*, 121, 14201–14220, <https://doi.org/10.1002/2016JD025142>, 2016.

758 Mattos, E. V., Machado, L. A. T., Williams, E. R., Goodman, S. J., Blakeslee, R. J., and Bailey, J.
759 C.: Electrification life cycle of incipient thunderstorms, *Journal of Geophysical Research:*
760 *Atmospheres*, 122, 4670–4697, <https://doi.org/10.1002/2016JD025772>, 2017.

761 Park, H. S., Ryzhkov, A. V., Zrnić, D. S., and Kim, K.: The Hydrometeor Classification Algorithm
762 for the Polarimetric WSR-88D: Description and Application to an MCS, *Weather and*
763 *Forecasting*, 24, 730–748, <https://doi.org/10.1175/2008WAF2222205.1>, 2009.

764 Pickering, K. E., Bucsela, E., Allen, D., Ring, A., Holzworth, R., and Krotkov, N.: Estimates of

765 lightning NO_x production based on OMI NO₂ observations over the Gulf of Mexico, *Journal*
766 *of Geophysical Research: Atmospheres*, 121, 8668–8691,
767 <https://doi.org/10.1002/2015JD024179>, 2016.

768 Qie, X., Yuan, S., Chen, Z., Wang, D., Liu D., Sun, M., Sun, Z., Srivastava, A., Zhang, H., Lu, J.,
769 Xiao, H., Bi, Y., Feng, L., Tian, Y., Xu, Y., Jiang, R., Liu, M., Xiao, X., Duan, S., Su, D., Sun,
770 C., Xu, W., Zhang, Y., Lu, G., Zhang, D., Yin, Y., and Yu, Y.: Understanding the
771 dynamical-microphysical-electrical processes associated with severe thunderstorms over the
772 Beijing metropolitan region, *Science China Earth Sciences*, 64, 10–26.
773 <https://doi.org/10.1007/s11430-020-9656-8>, 2021.

774 Ramachandran, R., Detwiler, A., Helsdon, J., Smith, P. L., and Bringi, V. N.: Precipitation
775 development and electrification in Florida thunderstorm cells during Convection and
776 Precipitation/Electrification Project, *Journal of Geophysical Research: Atmospheres*, 101,
777 1599–1619, <https://doi.org/10.1029/95JD02931>, 1996.

778 Reynolds, S. E., and Brook, M.: CORRELATION OF THE INITIAL ELECTRIC FIELD AND
779 THE RADAR ECHO IN THUNDERSTORMS, *Journal of the Atmospheric Sciences*, 13,
780 376–380, [https://doi.org/10.1175/1520-0469\(1956\)013<0376:COTIEF>2.0.CO;2](https://doi.org/10.1175/1520-0469(1956)013<0376:COTIEF>2.0.CO;2), 1956.

781 Reynolds, S. E., Brook, M., and Gourley, M. F.: Thunderstorm charge separation, *Journal of the*
782 *Atmospheric Sciences*, 14, 426–436,
783 [https://doi.org/10.1175/1520-0469\(1957\)014<0426:TCS>2.0.CO;2](https://doi.org/10.1175/1520-0469(1957)014<0426:TCS>2.0.CO;2), 1957.

784 Rosenfeld, D.: TRMM observed first direct evidence of smoke from forest fires inhibiting rainfall,
785 *Geophysical Research Letters*, 26, 3105–3108, <https://doi.org/10.1029/1999GL006066>, 1999.

786 Rosenfeld, D., Lohmann, U., Raga, G. B., O’Dowd, C. D., Kulmala, M., Fuzzi, S., Reissell, A.,
787 and Andreae, M. O.: Flood or drought: How do aerosols affect precipitation? *Science*, 321,
788 1309–1313, doi:10.1126/science.1160606, 2008.

789 Ryzhkov, A. V., Zhuravlyov, V. B., and Rybakova, N. A.: Preliminary results of X-band
790 polarization radar studies of clouds and precipitation, *Journal of Atmospheric and Oceanic*
791 *Technology*, 11, 132–139,
792 [https://doi.org/10.1175/1520-0426\(1994\)011<0132:PROXBP>2.0.CO;2](https://doi.org/10.1175/1520-0426(1994)011<0132:PROXBP>2.0.CO;2), 1994.

793 Saunders, C.: Charge Separation Mechanisms in Clouds, *Space Science Reviews*, 137, 335–353,
794 <https://doi.org/10.1007/s11214-008-9345-0>, 2008.

795 Saunders, C. P. R., Keith, W. D., and Mitzeva, R. P.: The effect of liquid water on thunderstorm
796 charging, *Journal of Geophysical Research*, 96, 11007–11017,
797 <https://doi.org/10.1029/91JD00970>, 1991.

798 Scharfenberg, K. A., Miller, D. J., Schuur, T. J., Schlatter, P. T., Giangrande, S. E., Melnikov, V. M.,
799 Burgess, D. W., Andra, D. L., Foster, M. P. Jr., and Krause, J. M.: The Joint Polarization
800 Experiment: Polarimetric Radar in Forecasting and Warning Decision Making, *Weather and*
801 *Forecasting*, 20, 775–788, <https://doi.org/10.1175/WAF881.1>, 2005.

802 Seliga, T. A., and Bringi, V. N.: Potential Use of Radar Differential Reflectivity Measurements at
803 Orthogonal Polarizations for Measuring Precipitation, *Journal of Applied Meteorology and*
804 *Climatology*, 15, 69–76,
805 [https://doi.org/10.1175/1520-0450\(1976\)015<0069:PUORDR>2.0.CO;2](https://doi.org/10.1175/1520-0450(1976)015<0069:PUORDR>2.0.CO;2), 1976.

806 Shi, D., Zheng, D., Zhang, Y., Zhang, Y. J., Huang, Z., and Lyu, W.: Low-frequency E-field
807 Detection Array (LFEDA)-Construction and preliminary results, *Science China Earth*
808 *Sciences*, 60, 1896–1908, <https://doi.org/10.1007/s11430-016-9093-9>, 2017.

809 Smith, P. L., Musil, D. J., Detwiler, A. G., and Ramachandran, R.: Observations of Mixed-Phase
810 Precipitation within a CaPE Thunderstorm, *Journal of Applied Meteorology and Climatology*,
811 38, 145–155, [https://doi.org/10.1175/1520-0450\(1999\)038<0145:OOMPPW>2.0.CO;2](https://doi.org/10.1175/1520-0450(1999)038<0145:OOMPPW>2.0.CO;2),
812 1999.

813 Snyder, J. C., Ryzhkov, A. V., Kumjian, M. R., Khain, A. P., and Picca, J. C.: A ZDR column
814 detection algorithm to examine convective storm updrafts, *Weather and Forecasting*, 30,
815 1819–1844, <https://doi.org/10.1175/WAF-D-15-0068.1>, 2015.

816 Stolzenburg, M., Marshall, T. C., and Krehbiel, P. R.: Initial electrification to the first lightning
817 flash in New Mexico thunderstorms, *Journal of Geophysical Research: Atmospheres*, 120,
818 11,253–11,276, <https://doi.org/10.1002/2015JD023988>, 2015.

819 Stolzenburg, M., Marshall, T. C., and Rust, W. D.: Serial sounding of electric field through a
820 mesoscale convective system, *Journal of Geophysical Research: Atmospheres*, 106,
821 12371–12380, <https://doi.org/10.1029/2001JD900074>, 2001.

822 Stough, S. M., and Carey, L. D.: Observations of anomalous charge structures in supercell
823 thunderstorms in the Southeastern United States, *Journal of Geophysical Research:*
824 *Atmospheres*, 125, e2020JD033012, <https://doi.org/10.1029/2020JD033012>, 2020.

825 [Stough, S. M., Carey, L. D., Schultz, C. J., and Cecil, D. J.: Examining conditions supporting the](#)
826 [development of anomalous charge structures in supercell thunderstorms in the Southeastern](#)
827 [United States, *Journal of Geophysical Research: Atmospheres*, 126, e2021JD034582,](#)
828 <https://doi.org/10.1029/2021JD034582>, 2021.

829 Takahashi, T.: Riming electrification as a charge generation mechanism in thunderstorms, *Journal*
830 *of the Atmospheric Sciences*, 35, 1536–1548,
831 [https://doi.org/10.1175/1520-0469\(1978\)035<1536:REAACG>2.0.CO;2](https://doi.org/10.1175/1520-0469(1978)035<1536:REAACG>2.0.CO;2), 1978.

832 Takahashi, T., Tajiri, T., and Sonoi, Y.: Charges on Graupel and Snow Crystals and the Electrical
833 Structure of Winter Thunderstorms, *Journal of the Atmospheric Sciences*, 56, 1561–1578,
834 [https://doi.org/10.1175/1520-0469\(1999\)056<1561:COGASC>2.0.CO;2](https://doi.org/10.1175/1520-0469(1999)056<1561:COGASC>2.0.CO;2), 1999.

835 Takahashi, T., Sugimoto, S., Kawano, T., and Suzuki, K.: Riming Electrification in Hokuriku
836 Winter Clouds and Comparison with Laboratory Observations, *Journal of the Atmospheric*
837 *Sciences*, 74, 431–447, <https://doi.org/10.1175/JAS-D-16-0154.1>, 2017.

838 Takahashi, T., Sugimoto, S., Kawano, T., and Suzuki, K.: Microphysical structure and lightning
839 initiation in Hokuriku winter clouds, *Journal of Geophysical Research: Atmospheres*, 124,
840 13156–13181, <https://doi.org/10.1029/2018JD030227>, 2019.

841 Tuttle, J. D., Bringi, V. N., Orville, H. D., and Kopp, F. J.: Multiparameter radar study of a
842 microburst: Comparison with model results, *Journal of the Atmospheric Sciences*, 46,
843 601–620, [https://doi.org/10.1175/1520-0469\(1989\)046<0601:MRSOAM>2.0.CO;2](https://doi.org/10.1175/1520-0469(1989)046<0601:MRSOAM>2.0.CO;2), 1989.

844 Uman, M. A., and Krider, E. P.: Natural and artificially initiated lightning, *Science*, 246, 457–464,
845 doi:10.1126/science.246.4929.457, 1989.

846 Vincent, B. R., Carey, L. D., Schneider, D., Keeter, K., and Gonski, R.: Using WSR-88D
847 reflectivity data for the prediction of cloud-to-ground lightning: A central North Carolina
848 study, *National Weather Digest*, 27, 35–44, 2003.

849 Woodard, C. J., Carey, L. D., Petersen, W. A., and Roeder, W. P.: Operational utility of
850 dual-polarization variables in lightning initiation forecasting, *Electronic J. Operational*
851 *Meteor.*, 13, 79–102, 2012.

852 Workman, E. J., and Reynolds, S. E.: Electrical activity as related to thunderstorm cell growth,
853 *Bulletin of the American Meteorological Society*, 30, 142–149,
854 <https://doi.org/10.1175/1520-0477-30.4.142>, 1949.

855 Wu, C., Liu, L., Wei, M., Xi, B., and Yu, M.: Statistics-based optimization of the polarimetric
856 radar hydrometeor classification algorithm and its application for a squall line in South China,
857 *Advances in Atmospheric sciences*, 35, 296–316, <https://doi.org/10.1007/s00376-017-6241-0>,
858 2018.

859 Zhang, Y., Lyu, W., Chen, S., Zheng, D., Zhang, Y., Yan, X., Chen, L., Dong, W., Dan, J., and Pan,
860 H.: A review of advances in lightning observations during the past decade in Guangdong,
861 China, *Journal of Meteorological Research*, 30, 800–819,
862 <https://doi.org/10.1007/s13351-016-6928-7>, 2016.

863 Zhang, Y. J., Yan, M., Sun, A., and Guo, F.: Thunderstorm electricity. *China Meteorological Press*,
864 384 pp., 2009.

865 Zhang, Y. J., Sun, A., Yan, M., Guo, F., Qie, X., and Huang, M.: Numerical Simulations of the
866 Effects of Electric Environment on Hail Growth, *Chinese Journal of Geophysics*, 47, 29–37,
867 <https://doi.org/10.1002/cjg2.451>, 2004.

868 Zhao, C.: Data for “[On the ice microphysics of isolated thunderstorms and non-thunderstorms in](#)
869 [southern China: A radar polarimetric perspective](#)~~Microphysical characteristics of the first~~
870 ~~lightning flash occurrence within isolated warm season thunderstorms over South China~~”.
871 Figshare. [Dataset]. <https://doi.org/10.6084/m9.figshare.22718437.v5.v6>, 2024.

872 Zhao, C., Zhang, Y. J., Zheng, D., Liu, X., Zhang, Y., Fan, X., Yao, W., and Zhang, W.: Using
873 polarimetric radar observations to characterize first echoes of thunderstorms and
874 nonthunderstorms: A comparative study, *Journal of Geophysical Research: Atmospheres*, 127,
875 e2022JD036671, <https://doi.org/10.1029/2022JD036671>, 2022.

876 Zhao, C., Zhang, Y. J., Zheng, D., Zhou, Y., Xiao, H., and Zhang, X.: An improved hydrometeor
877 identification method for X-band dual-polarization radar and its application for one summer
878 Hailstorm over Northern China, *Atmospheric Research*, 245, 105075,
879 <https://doi.org/10.1016/j.atmosres.2020.105075>, 2020.

880 Zhao, C., Zheng, D., Zhang, Y. J., Liu, X., Zhang, Y., Yao, W., and Zhang, W.: Turbulence
881 Characteristics before the Occurrence of the First Flash in Thunderstorms and
882 Non-Thunderstorms, *Geophysical Research Letters*, 48, e2021GL094821,
883 <https://doi.org/10.1029/2021GL094821>, 2021a.

884 Zhao, C., Zheng, D., Zhang, Y. J., Liu, X., Zhang, Y., Yao, W., and Zhang, W.: Characteristics of

885 cloud microphysics at positions with flash initiations and channels in convection and
886 stratiform areas of two squall lines, *Journal of Tropical Meteorology*, 37, 358–369,
887 doi:10.16032/j.issn.1004-4965.2021.035, 2021b.

888 Zheng, D., Zhang, Y., Zhang, Y., Lyu, W., Chen, L., and Shi, D.: Lightning activity characteristics
889 as indicated by lightning location systems in Guangdong, in: *1st International Workshop of*
890 *the Southern China Monsoon Rainfall Experiment (SCMREX), Beijing, China*, 12–13 April,
891 2017.

892 [Zipser, E. J., Cecil, D. J., Liu, C., Nesbitt, S. W. and Yorty, D. P.: WHERE ARE THE MOST](#)
893 [INTENSE THUNDERSTORMS ON EARTH? *Bulletin of the American Meteorological*](#)
894 [Society, 87, 1057–1072, <https://doi.org/10.1175/BAMS-87-8-1057>, 2006.](#)

895 Zrnica, D. S., and Ryzhkov, A. V.: Polarimetry for Weather Surveillance Radars, *Bulletin of the*
896 *American Meteorological Society*, 80, 389–406,
897 [https://doi.org/10.1175/1520-0477\(1999\)080<0389:PFWSR>2.0.CO;2](https://doi.org/10.1175/1520-0477(1999)080<0389:PFWSR>2.0.CO;2), 1999.

898

899 **Authors contributions**

900 Conceptualization: C. Zhao, Y. Zhang

901 Data curation: C. Zhao, Y. Zhang, D. Zheng, S. Du, and X. Liu

902 Formal analysis: C. Zhao, Y. Zhang, H. Li, X. Peng, P. Zhao, J. Zheng, and J. Shi

903 Funding acquisition: Y. Zhang, C. Zhao

904 Investigation: C. Zhao, Y. Zhang

905 Methodology: C. Zhao, Y. Zhang, and H. Li

906 Project Administration: Y. Zhang

907 Resources: C. Zhao, Y. Zhang

908 Software: C. Zhao, D. Zheng

909 Supervision: Y. Zhang

910 Validation: C. Zhao, Y. Zhang

911 Visualization: C. Zhao, Y. Zhang, and H. Li

912 Writing-original draft: C. Zhao, Y. Zhang, X. Peng, and H. Li

913 **Competing interests**

914 The contact author has declared that none of the authors has any competing interests.

915